SLAC–PUB–6374
October 1993
(T/E)

Threshold inelastic electron scattering from the proton at high momentum transfers*

P. E. Bosted, R. G. Arnold, C. C. Chang,[a] J. Gomez,[c]
P A. T. Katramatou, C. J. Martoff[b], G. G. Petratos,[d]
A. A. Rahbar, S. E. Rock, A. F. Sill,[e] Z. M. Szalata

Department of Physics, The American University, Washington, DC 20016

D. J. Sherden

Stanford Linear Accelerator Center, Stanford, California 94309

J. M. Lambert

Department of Physics, Georgetown University, Washington DC 20056

R. M. Lombard-Nelsen

CE-Saclay, DAPNIA/SphN, F-91191 Gif-sur-Yvette, France

ABSTRACT

Cross sections for threshold electron scattering from the proton have been measured in the missing-mass squared region $M^2 < W^2 < 2$ (GeV)^2 and the four-momentum transfer squared region $6 < Q^2 < 30$ (GeV/c)^2. Scaling of the extracted values of the structure function $F_2 = \nu W_2$ is examined in the variables x, ξ, and W^2. The best scaling is found for the quantity $Q^6 F_2$, which is found to be linearly proportional to $(W^2 - W_{\rm th}^2)$, where $W_{\rm th} = M + M_\pi$.

Submitted to Physical Review D

* Work supported in part by Department of Energy contract DE–AC03–76SF00515 (SLAC) and National Science Foundation grants PHY–85–10548 and PHY–91–14958 (American). R. M. Lombard–Nelsen was supported by C.N.R.S. (French National Center for Scientific Research). J. Gomez was partially supported by CONICIT, Venezuela.

I. INTRODUCTION

Inelastic electron scattering from a nucleon at large four-momentum transfer squared Q^2 has been successfully used to study the longitudinal quark momentum distributions. The deep inelastic structure functions $F_2(x,Q^2) = \nu W_2(x,Q^2)$ and $F_1(x,Q^2) = MW_1(x,Q^2)$ become approximately independent of Q^2 at fixed x, in a phenomenon known as scaling, for $Q^2 > 2$ (GeV/c)^2 and $W^2 > 4$ (GeV)^2. The x variable is a measure of the longitudinal momentum carried by the struck partons, and is kinematically defined as $x = Q^2/2M\nu$, where M is the nucleon mass, $\nu = E - E'$ is the energy transferred by an electron of initial energy E and final energy E', and Q^2 is related to the electron scattering angle θ through the relation $Q^2 = 4EE'\sin^2(\theta/2)$. The mass of the final state squared is given by $W^2 = M^2 + 2M\nu - Q^2$. Logarithmic scaling violations are well-described by perturbative QCD (pQCD), while at low Q^2 corrections proportional to $1/Q^2$ are needed to account for target-mass and higher twist effects. For $W^2 < 4$ (GeV)^2, various nucleon resonances become important, but Bloom and Gilman [1] found that the resonance form factors averaged over a finite range in x fall at the approximately same rate as the deep inelastic structure functions. This local duality was shown [2] to follow from pQCD, even for the nucleon elastic peak at $x = 1$. It was also demonstrated that the effect of the finite target mass can be removed by analyzing the structure functions in terms of the Nachtmann variable $\xi = 2x/[1 + (1 + 4M^2x^2/Q^2)^{1/2}]$, which approaches x at high Q^2.

In both a simple parton picture and in a more sophisticated QCD analysis [3], the structure functions F_1 and F_2 are expected to behave near threshold approximately as $(1-x)^3$ [or equivalently $(1-\xi)^3$] when averaged over the resonances, at sufficiently high Q^2. While this relation is known to be approximately valid,

both the x and ξ variables do not take into account the fact that the threshold for inelastic scattering is not at $W^2 = M^2$ ($x = 1$), but actually occurs at $W^2_{\rm th} = (M + M_\pi)^2 \approx 1.16$ (GeV/c)^2, or $x = [1 + (2MM_\pi + M_\pi^2)/Q^2]^{-1}$, where M_π is the pion mass. In this paper we will examine the scaling behavior of threshold inelastic cross sections, and propose that the most useful variable for these studies is the missing mass W^2.

Most of the data comes from the analysis of an experiment [4,5] that was primarily designed to measure elastic electron scattering from the proton at very high momentum transfers, up to 31 (GeV/c)^2. The next sections gives details of the analysis of the inelastic data, while Section III shows the results of the scaling studies. Conclusions are given in Section IV.

II. THE EXPERIMENT

The new data for this analysis comes from SLAC experiment E136 [4,5]. While the primary goal of this experiment was to measure elastic scattering, the spectrometer bite of $\pm 4\%$ was large enough to accept electrons in the threshold inelastic region as well, with a maximum W^2 of 1.5 to 2 (GeV)^2, where the maximum value increased with increasing Q^2. A brief overview of the experimental apparatus is given below, followed by a description of the radiative corrections used to obtain the threshold inelastic cross sections. Additional experimental details can be found in Ref. [5].

A. Beam and Target

The electron beam energy E ranged from 5 to 21.5 GeV, with typically 4×10^{11} electrons per pulse at a repetition rate of 180 Hz. The energy spread was limited

to $\pm 0.2\%$ by collimators. The beam current was measured with an accuracy of $\pm 0.5\%$ by a pair of independent toroidal coils forming resonant circuits. The beam position was monitored with a pair of thin wire arrays upstream of the target, and the beam position was stabilized with computer-controlled feedback to a set of steering magnets. The principal target was a 65-cm-long cylinder filled with circulating liquid hydrogen maintained at a pressure of 2 atm and a temperature of 21 K. The circulation speed was high enough to prevent local density changes due to the formation of bubbles along the beam path. The average temperature and pressure were monitored with both platinum resistors and with vapor pressure bulbs. The most important innovation for this experiment was the use of a set of two tungsten shields placed between the aluminum target endcaps and the first magnet of the spectrometer. Electrons scattering from the endcaps were effectively stopped. This was especially important at high Q^2, where contributions from even thin aluminum endcaps would have been substantial in the threshold region due to the increasing effects of Fermi smearing of the cross sections.

B. Spectrometer and Detectors

Electrons scattered from the target were detected in the SLAC 8 GeV/c spectrometer, which was set at a central electron scattering angles θ of 21° for most of the data points. Due to the maximum beam energy of 21.5 GeV, scattering angles of 25° and 33° were used for the two highest Q^2 points of 27 and 31 $(\mathrm{GeV/c})^2$ respectively. Averaged over the visible target length, the solid angle of the spectrometer was about 0.5 msr, with a momentum acceptance of $\pm 4\%$ and a relative momentum resolution of about 0.05%. Combined with a θ resolution of about 0.1 mr, this led to a resolution in W^2 of from 0.01 $(\mathrm{GeV})^2$ at low Q^2 to 0.03 $(\mathrm{GeV})^2$

at high Q^2. A detailed model of the acceptance was made using deep-inelastic electron scattering, where the variation of cross section with E' and θ is well known and smooth, combined with Monte Carlo simulation based on the known optical properties of the magnets.

The detector package was designed to determine particle trajectories and to distinguish electrons from a large flux of pions and other backgrounds. It included a 2.8 m long, 99% efficient gas Čerenkov counter filled with 0.4 to 0.6 atm of nitrogen and a 98% efficient lead glass shower counter array with a resolution of $\pm 8.5\%/\sqrt{E'}$. The lead glass array was segmented longitudinally into a 3 r.l. preradiator and a 16.8 r.l. total absorber. These detectors together provided a pion rejection power of about 1:10,000, more than adequate to essentially eliminate all pions from the elastic spectra. Ten planes of multi-wire proportional chambers were used to measure particle track coordinates with an efficiency of 99.9%.

C. Threshold Inelastic Spectra

Spectra at each kinematic point were obtained as a function of W^2 at fixed θ by dividing the measured counts by the acceptance and correcting for the cross-section variation within the small ± 8 mr $\delta\theta$ range of the spectrometer. The kinematics were fairly well-defined for each point, since the overall uncertainties in E, E', and θ were 0.1%, 0.1%, and 0.01° respectively. Small corrections to the nominal beam energy were made to center the elastic peaks at $W^2 = M^2$, after accounting for the shift in the peak position expected from radiative corrections. The raw spectra are shown in Fig. 20 of Ref. [5]. The final experimental cross sections were obtained by applying corrections for radiative processes, using the peaking approximation formulas of Tsai [6], with improvements [7] to account for μ, τ, and quark vacuum

loops, higher order terms in the fine-structure constant α, and radiation from quarks. Another important improvement was the inclusion of the Q^2 dependence of the elastic cross section [8]. The peaking approximation is expected to be valid at the 1% to 2% level in our kinematic region, so the full formulas which integrate over all emitted photon angles were not used. The contribution from the elastic tail was 100% exactly at threshold (by definition), decreasing to typically 20% at $W^2 = 1.5$ (GeV)^2 and 10% at $W^2 = 2$ (GeV)^2. For the inelastic radiative corrections, several iterations were made over the input model cross sections until reasonable convergence was achieved. The final model used was given by

$$F_2^{\rm mod} \;=\; [3.5\ ({\rm Gev})^4]\ Q^{-6}\ \ (W^2 - W_{\rm th}^2)\ , \tag{2.1}$$

where $W_{\rm th}^2 = (M + M_\pi)^2 \approx 1.16$ (GeV)^2. This fit is shown in Figs. 1 and 2, along with the data at each of the kinematic points. The fit provides a good description of the data at all measured values of Q^2 and W^2. The data have been converted from experimental cross sections to values of F_2 using the relation

$$F_2 \;=\; \frac{\nu\sigma(E,E',\theta)}{\sigma_M}\left[1 + 2\left(1 + \frac{\nu^2}{Q^2}\right)\frac{\tan^2(\theta/2)}{(1+R)}\right]^{-1}\ , \tag{2.2}$$

where the Mott cross section is given by $\sigma_M = [2\alpha E' \cos(\theta/2)/Q^2]^2$, and for $R = \sigma_L/\sigma_T$ we used the relation $R = [0.32\ ({\rm GeV/c})^2]/Q^2$. This parametrization, which is essentially zero for most of our high Q^2 data, is in reasonable agreement with the limited data available near $x = 1$ [9]. The use of a constant value $R = 0.18$, which was used in previous experiments [10], is now considered unreasonable because it does not go to zero at high Q^2. If we were to make this assumption, the effect would be largest at the highest Q^2, reducing the values of νW_2 by 10%. In all

cases, the effect is much smaller than the statistical errors. The final cross section and extracted values of F_2 are listed in Table I.

III. SCALING AND THE ELASTIC-INELASTIC CONNECTION

There are several ways to look for patterns in the measured structure functions. In the simple parton model picture, the structure functions should depend on only $x = Q^2/2M\nu$, which, in this picture, is the fractional longitudinal momentum of the struck parton. pQCD can then be used to describe the logarithmic evolution with Q^2. Related scaling variables, such as x' and ξ, have been used in the past to effectively account for corrections such as finite target mass effects, dynamic higher twist, and the coherent resonances. We will consider the x, ξ, and W^2 variables in the following sections.

A. x scaling

In the parton model [3], it is expected that F_2 should behave as $(1-x)^3$ at high x, since there are two spectator quarks. This model is closely related to the form factor scaling model, which successfully predicts [4] that G_{Mp} should fall as $(1/Q^2)^2$, again under the assumption that the principal interaction takes place with a single high x valence quark, with two hard gluon exchanges taking place to keep the nucleon bound. In light-cone QCD perturbation theory [11, 12], there are several corrections to the simple $(1-x)^3$ form. The first is a factor of $\alpha_s^4(k_x^2)$, where $|k_x|^2 \sim O(M^2/(1-x))$. Including the wave function anomalous dimension introduces a logarithmic dependence on k_x, and including gluon radiation introduces a Q^2 evolution function $P(x,Q^2)$. For x near 1, $P(x,Q^2)$ is expected [11] to have a form $(1-x)^{\Delta\bar{\xi}}$, where $\Delta\bar{\xi}$ depends on log[log(Q^2)], and varies from about 0.6 to 0.8 for Q^2 from 6 to 30 (GeV/c)^2. Thus the leading-twist prediction from

perturbative QCD would be an x-dependence of approximately $(1-x)^{3.7}$ in our Q^2 region, with an overall magnitude that changes only as $\log(Q^2)$. However, since at x near 1 we are in a coherent region where the quarks are forced to be nearly colinear, higher twist contributions are likely to be as large at fixed W^2 as leading twist contributions. According to [11], the higher twist contributions should have about the same Q^2 evolution as the leading twist (LT) contribution, and should give corrections of the form

$$F_2 \propto F_2^{(LT)} \left[1 + \frac{A\mu^2}{Q^2(1-x)} + \frac{B\mu^4\alpha_s^{-1}\,(k_x^2)}{Q^4(1-x)^2} + \cdots\right], \qquad (3.1)$$

where $\mu^2 \sim O(M^2)$ is set by the wave function scale, and A and B are dimensionless parameters. These higher-twist terms could then cause a substantial falloff of F_2 with increasing Q^2 at fixed x.

As can be seen from the data plotted in Fig. 3, there does seem to be fairly good scaling in x, with a tendency for F_2 to decrease with increasing Q^2 at fixed x, as expected from higher-twist and Q^2 evolution effects. In addition to the data from the present experiment, we have included three high-statistics spectra from a previous SLAC experiment [13] at mean Q^2 values of 5.9, 7.9, and 9.8 (GeV/c)^2. Note that an error was recently discovered in the sign of the corrections to the beam energies in Table 1 of Ref. [13]. After subtracting 6 MeV to obtain the average energy at the center of the target, the corrected energies are 9.766, 12.601, 15.742, 18.506, and 20.991 GeV for the spectra at nominal Q^2 values of 2.5, 4, 6, 8, and 10 (GeV/c)^2, respectively. While the corrected energies are only a few tenths of a percent different from the old ones, the effect close to threshold is quite significant due to the resulting shift in the W^2 scale, or equivalently in the x scale.

The solid line in Fig. 3 is a simple fit given by $F_2(x,Q^2) = 5.0(1-x)^3$, which has the expected spectator power law behavior. The largest deviations from this fit comes from the lowest Q^2 spectrum [solid diamonds, $Q^2 = 5.9$ (GeV/c)^2]. The deviation near $x = 0.9$ is from the $\Delta(1232)$ resonance. As has been well-documented [14], mainly based on the data of [13], the $\Delta(1234)$ resonance form factor is unusual in that it falls faster with Q^2 (going as Q^{-6}) than the elastic channel or the prominent resonances at higher W^2 (which fall as Q^{-4}). Since the Δ has virtually disappeared into the background for $Q^2 = 8$ (GeV/c)^2 and above, and there are no other prominent resonances below $W^2 = 2$ (GeV)^2, it is not too surprising that the remaining spectra in Fig. 3 show a smooth behavior with x.

Another obvious deviation from the scaling at low Q^2 is caused by the threshold effect. Since the threshold goes as

$$x_{\rm th} = \left[1 + \frac{W_{\rm th}^2 - M^2}{Q^2}\right]^{-1} \approx 1 - \frac{0.28}{Q^2}\,, \tag{3.2}$$

and since by definition $F_2 = 0$ above $x_{\rm th}$, scaling must break down in this kinematic region. This is most apparent in the $Q^2 = 5.9$ (GeV/c)^2 spectrum. Interestingly, at higher Q^2, this threshold effect is small enough to not be observable within the rather large statistics of our data. One way to get around the threshold problem is to plot the data as a function of $x_{\rm th} - x$. However, when we did this, we found much worse scaling than from simply plotting the data versus x (a factor a five spread in the data instead of a factor of two).

As suggested in a recent paper [15], it is of interest to compare the magnitude of data to some of the commonly used parametrizations. In the quark-parton model, F_2 is related to the quark distribution functions by $F_2 = \frac{x}{9}\left[4u_v(x) + d_v(x)\right]$,

where $u_v(x)$ and $d_v(x)$ are the up- and down-quark valence distributions respectively, and we have neglected sea quark distributions since we are only interested in the region near $x = 1$. Also, the ratio $d_v(x)/u_v(x)$ is known to be small [10] at high x, and considering the factor of 4 multiplying $u_v(x)$ (due to the quark charge squared), to a good approximation $F_2 = x\frac{4}{9}u_v(x)$. One commonly used parametrization [16] is given by $u_v(x) = 0.73\,x^{0.36}(1-x)^{3.7}(1+11.86\,x)$. This is shown as the dashed curve in Fig. 3, and although it has about the correct shape, it lies about a factor of five below the data. Another recent fit [17] has $u_v(x) = 2.40\,x^{0.60}(1-x^{1.4})^{3.1}$. As can be seen from the dotted curve, it lies about a factor of two below the data, although again with about the right x-dependence. Since these fits are essentially extrapolations of lower x data (the only available data for $x > 0.85$ is in the resonance region, and hence was not included in the fits), it is not surprising that the magnitude of these fits is in disagreement with the data. The observation that the data lies above these extrapolations could be another indication of the importance of higher twist contributions.

B. ξ scaling

It has been common to use the Nachtmann [18] variable

$$\xi = \frac{2x}{1+\sqrt{1+4M^2x^2/Q^2}} \tag{3.3}$$

instead of x because it is expected to approximately account for target mass effects, and seems to give better scaling than x in the resonance region. However, plotting $F_2(x,Q^2)$ as a function of ξ results in very poor scaling when only data close to threshold is considered, because the kinematic threshold shift is a much bigger effect than if x is used. As shown in Fig. 4, approximate scaling can be restored

if the data is instead plotted as a function of $(\xi - \xi_{\rm max})$, where $\xi_{\rm max}$ is obtained by using $x = 1$ in Eq. (3.3). Scaling in the threshold region ($\xi - \xi_{\rm max} > -0.05$ is almost as good as was obtained using x as the scaling variable, but a larger spread is seen at lower ξ. It is hard to know what conclusion to draw from this. Assuming that it is indeed valid to replace ξ with $(\xi - \xi_{\rm max})$ as a scaling variable, it could be that the somewhat worse scaling compared to using x is simply better evidence of coherence and higher twist effects, which would explain the clear trend of the data to decrease with increasing Q^2 at fixed $(\xi - \xi_{\rm max})$.

C. Scaling of Q^6F_2 versus W^2

The easiest and most appealing way to avoid the problem of the threshold for inelastic scattering changing with Q^2 is to use the variable W^2, rather than x or ξ. In this variable, the threshold is always fixed at $W^2_{\rm th} = (M+M_\pi)^2 \approx 1.16\ ({\rm GeV/c})^2$, and the position of the various resonances is also held fixed. As illustrated in Fig. 5, we have found that multiplying the extracted values of $F_2(x, Q^2)$ by Q^6 produces remarkably good scaling. Except for the lowest Q^2 spectrum ($Q^2 = 5.9$, solid diamonds), which is a little bit low above $W^2 = 1.6\ ({\rm GeV})^2$, all the data are consistent with a simple linear fit of the form given in Eq. (2.1). A more quantitative examination of the Q^2 dependence is illustrated in Fig. 6, where we have plotted the integral of Q^6F_2 from threshold to three maximum values of W^2 as a function of Q^2. The integrals have significantly smaller errors than the individual data points, making it easier to see the Q^2-dependence. Two additional low Q^2 spectra from [13] have been included. For all three ranges of W^2, the integrals increase with Q^2 at first, then become constant above $Q^2 = 6\ ({\rm GeV/c})^2$, indicating good W^2 scaling for Q^6F_2. The dashed lines indicate the integrated values of the simple fit shown in Eq. (2.1). We also examined the resonance region data shown

in Ref. [10], which goes up to $Q^2 = 21$ (GeV/c)^2. Within the much larger errors of this data set, the integrated results are consistent with those shown in Fig. 6.

While this Q^6F_2 scaling must begin to break down at $W^2 > 4$ (GeV)^2, since F_2 becomes more-or-less independent of Q^2 in the deep-inelastic region, the question remains as to why it seems to work so well near threshold. One way to examine this is the connection with the expected power law dependence in $(1-x)$ discussed above in Section III.A. If we take just a leading twist $(1-x)^3$ behavior and rewrite

$$(1-x)^3 \;=\; x^3\left(\frac{W^2-M^2}{Q^2}\right)^3 , \tag{3.4}$$

the observed Q^{-6} behavior can readily be understood. However, the predicted $(W^2-M^2)^3$ dependence has the problem of predicting a nonzero cross section below threshold, and even above threshold does not provide as good a quantitative description as the linear dependence on $W^2 - W_{\rm th}^2$ evident in the data shown in Fig. 5. A linear dependence on $W^2 - W_{\rm th}^2$ could be thought of as a minimal description of increasing available phase space with increasing W^2. It is interesting to note that the inclusion of higher twist contributions as in Eq. (3.1) preserves the prediction of Q^{-6} behavior. For example, considering the term proportional to B, we would have

$$F_2 \;=\; F_2^{LT}\,\frac{B\mu^4\alpha_s^{-1}(k_x^2)}{Q^4(1-x)^2} \;\approx\; \frac{(1-x)}{Q^4} \;\approx\; x\,\frac{(W^2-M^2)}{Q^6} , \tag{3.5}$$

which now gives a linear dependence on W^2, while still preserving the Q^{-6} dependence. If M^2 could be replaced by $W_{\rm th}^2$ in Eq. (3.5), this higher twist term would give a very good representation of the data.

Another way to understand the Q^{-6} dependence of F_2 at fixed W^2 is in terms of an elastic-inelastic connection based on correspondence arguments [19]. In this picture, which is closely related to duality arguments, threshold inelastic scattering can be thought of as a series of nearly elastic scattering to a continuous series of final states of mass squared W^2. At forward angles and large Q^2, the elastic scattering cross section is essentially given by

$$\sigma_{\rm el} \approx \sigma_M \frac{E'}{E} G^2_{Mp}(Q^2) . \tag{3.6}$$

When integrated over a small finite region in W^2, the threshold inelastic cross section is given by

$$\sigma_{\rm th} \approx \sigma_M \frac{E'}{E} \frac{\delta W^2}{2M} W_2(W^2, Q^2) . \tag{3.7}$$

Comparing these equations, there is a clear correspondence between W_2 and G^2_{Mp}, so that at fixed W^2 the ratio W_2/G^2_{Mp} should be a constant. Since to a very good approximation, G^2_{Mp} is proportional to Q^{-8}, and since at small values of W^2 and large values of Q^2, the quantity ν can be approximated by $\nu = Q^2/2M$, we have

$$W_2(W^2, Q^2)/G^2_{Mp}(Q^2) \propto Q^6 F_2(W^2, Q^2) . \tag{3.8}$$

Thus the observed Q^2–independence of $Q^6 F_2(W^2, Q^2)$ at fixed W^2 can be explained in terms of the expected scaling of W_2/G^2_{Mp} from the correspondence argument.

IV. SUMMARY

We have analyzed data for threshold inelastic scattering from the proton, providing a significant increase in the statistical precision available at very high Q^2.

Scaling of F_2 in the variables x and ξ was examined and found to work only at the factor of two level. Much better scaling behavior was found using W^2 as the scaling variable, and $Q^6F_2(W^2,Q^2)$ as the scaling quantity. The data for $Q^2 > 6$ (GeV/c)^2 are remarkably well described by a simple fit of the form $Q^6F_2(W^2,Q^2) = 3.5(W^2 - W_{\rm th}^2)$. The Q^{-6} behavior at fixed W^2 can be explained both in terms of correspondence arguments for the elastic-inelastic connection, and in terms of leading and higher twist contributions in pQCD. The observed simple linear dependence on $(W^2 - W_{\rm th}^2)$ is not readily predicted from current theories, but may indicate the importance of some fundamental feature of threshold inelastic scattering that more detail theoretical studies could help to define.

The $\Delta(1236)$ resonance has essentially disappeared in the region studied [$1.16 < W^2 < 2$ (GeV)^2]. The nonresonant background is following the Q^2 dependence expected from QCD ($W_2 = F_2/\nu \propto Q^{-8}$), which to some extent must mean that this region can be thought of as a series of closely spaced resonances, each falling with the same Q^2 dependence of both the elastic form factors and those of the principal higher mass resonances, such as the $S_{11}(1511)$. The challenge now is to understand this behavior in terms of more detailed models of nucleon. Specifically, it would be very nice to have a perturbative QCD prediction for the x and Q^2 dependence of F_2 that takes into account the finite threshold at $W^2 = (M + M_\pi)^2$. It would be even nicer to see predictions of the absolute magnitude of F_2 in the threshold region. Comparisons of such calculations with the present data may eventually help to shed light of the detailed valence structure of the proton.

ACKNOWLEDGMENTS

We wish to acknowledge the support of D. Brown, R. Eisele, J. Mark, J. Nicol, B. Smith, D. Tsang, and the rest of the SLAC staff, and valuable discussions with J. Bjorken, S. Brodsky, C. Carlson, and P. Stoler.

REFERENCES

[a] Permanent address: Department of Physics and Astronomy, University of Maryland, College Park, MD 20742.

[b] Present address: CEBAF, Newport News, VA 23606.

[c] Permanent address: Temple University, Philadelphia, PA 19122.

[d] Present address: SLAC, Stanford, CA 94309.

[e] Present address: Texas Tech University, Lubbock, TX 79409–1051.

1. E. Bloom and F. Gilman, Phys. Rev. **D4**, 2901 (1971).
2. A. De Rujula, H. Georgi, and H. D. Politzer, Ann. Phys. **103**, 315 (1977); H. Georgi and H. D. Politzer, Phys. Rev. **D14**, 1829 (1976); Phys. Rev. Lett. **36**, 1281 (1976).
3. S. D. Drell and T. M. Yen, Phys. Rev. Lett. **24**, 181 (1970); G. B. West, Phys. Rev. Lett. **24**, 1206 (1970); S. Brodsky and R. Blankenbecler, Phys. Rev. **D10**, 2973 (1974); G. R. Farrar and D. R. Jackson, Phys. Rev. Lett. **35**, 1416 (1975).
4. R. G. Arnold *et al.,* Phys. Rev. Lett. **57**, 174 (1986).
5. A. F. Sill *et al.,* Phys. Rev. **D48**, 29 (1993).
6. Y. S. Tsai, SLAC–PUB–848 Rev. (1971); see also L. W. Mo and Y. S. Tsai, Rev. Mod. Phys. **41**, 205 (1969).
7. A. A. Akhundov, D. Yu. Bardin, and N. M. Shumeiko, Sov. J. Nucl. Phys. **44**, 988 (1986); **26**, 660 (1977).
8. R. C. Walker, PhD Thesis, California Institute of Technology, 1989.
9. P. Bosted *et al.,* Phys Rev. **C46**, 2505 (1992); L. W. Whitlow *et al.,* Phys. Lett. **B250**, 193 (1990).

10. A. Bodek *et al.*, Phys. Rev. **D20**, 1471 (1979).

11. S. J. Brodsky, in *Lectures on Lepton Nucleon Scattering and Quantum Chromodynamics*, Progress in Physics, Vol. 4, 1982, pp. 255–415,.

12. V. M. Balyaev and B. L. Ioffe, Nucl. Phys. **B310**, 548 (1988); Nucl. Phys. **B313**, 647 (1989).

13. S. E. Rock *et al.*, Phys Rev. **D46**, 24 (1992). See text for corrected incident beam energies.

14. P. Stoler, Phys. Rev. **D44**, 73 (1991); Phys. Rev. Lett. **66**, 1003 (1991).

15. C. Carlson and N. Mukhopadhyay, Phys. Rev. **D47**, 1737 (1993).

16. J. Morfin and W. K. Tung, Z. Phys. **C52**, 13 (1991).

17. E. Eichten, I. Hinchliffe, C. Quigg, Phys. Rev. **D45**, 2269 (1992).

18. O. Nachtmann, Nucl. Phys . **B63**, 237 (1973); **B78**, 455 (1974).

19. J. D. Bjorken and J. Kogut, Phys. Rev. **D8**, 1341 (1973).

Table I. Cross sections for threshold inelastic electron-proton scattering from this experiment. Also shown are values of F_2 extracted assuming $R = 0.32/Q^2$.

E' (GeV)	W^2 (GeV)^2	Q^2 (GeV/c)^2	x	$d\sigma/d\Omega dE'$ (pb/sr-GeV)	F_2 ($\times 10^3$)
		$E = 9.607$ GeV		$\theta = 21.010°$	
5.627	1.160	7.188	0.963	1.6 ± 4.8	0.11 ± 0.32
5.614	1.200	7.172	0.957	5.7 ± 4.0	0.38 ± 0.27
5.602	1.240	7.155	0.952	14.8 ± 4.0	0.99 ± 0.27
5.589	1.280	7.139	0.947	8.4 ± 3.4	0.56 ± 0.23
5.576	1.320	7.123	0.942	15.7 ± 3.7	1.06 ± 0.25
5.564	1.360	7.107	0.937	15.1 ± 3.6	1.02 ± 0.24
5.551	1.400	7.091	0.932	31.5 ± 4.3	2.14 ± 0.29
5.538	1.440	7.074	0.927	45.0 ± 4.8	3.06 ± 0.33
5.526	1.480	7.058	0.922	45.4 ± 4.8	3.09 ± 0.33
5.513	1.520	7.042	0.917	55.3 ± 5.2	3.77 ± 0.35
		$E = 11.454$ GeV		$\theta = 21.010°$	
6.236	1.175	9.497	0.970	2.5 ± 1.6	0.30 ± 0.19
6.223	1.220	9.477	0.965	-0.3 ± 1.0	-0.04 ± 0.12
6.209	1.265	9.457	0.961	4.2 ± 1.2	0.51 ± 0.14
6.196	1.310	9.437	0.956	4.6 ± 1.2	0.56 ± 0.14
6.183	1.355	9.416	0.952	4.5 ± 1.1	0.54 ± 0.14
6.170	1.400	9.396	0.948	11.4 ± 1.5	1.38 ± 0.18
6.156	1.445	9.376	0.943	10.3 ± 1.4	1.25 ± 0.17
6.143	1.490	9.356	0.939	11.6 ± 1.4	1.40 ± 0.17
6.130	1.535	9.336	0.934	15.4 ± 1.6	1.87 ± 0.19
6.117	1.580	9.316	0.930	17.5 ± 1.7	2.13 ± 0.21
6.104	1.625	9.295	0.926	17.7 ± 1.7	2.16 ± 0.21
		$E = 13.191$ GeV		$\theta = 21.010°$	
6.734	1.185	11.812	0.975	0.57 ± 0.73	0.11 ± 0.14
6.721	1.235	11.788	0.971	0.16 ± 0.56	0.03 ± 0.11
6.707	1.285	11.763	0.967	0.86 ± 0.58	0.16 ± 0.11
6.693	1.335	11.739	0.963	1.59 ± 0.61	0.30 ± 0.12
6.679	1.385	11.715	0.959	2.49 ± 0.67	0.48 ± 0.13
6.665	1.435	11.691	0.955	3.81 ± 0.76	0.73 ± 0.15
6.652	1.485	11.667	0.951	3.89 ± 0.76	0.75 ± 0.15
6.638	1.535	11.643	0.947	3.98 ± 0.76	0.76 ± 0.15
6.624	1.585	11.619	0.943	6.66 ± 0.93	1.28 ± 0.18
6.610	1.635	11.594	0.939	7.13 ± 0.96	1.37 ± 0.18

Continued

Table I. Continued.

E' (GeV)	W^2 (GeV)^2	Q^2 (GeV/c)^2	x	$d\sigma/d\Omega dE'$ (pb/sr-GeV)	F_2 ($\times 10^3$)
		$E = 15.838$ GeV		$\theta = 21.010°$	
7.393	1.158	15.569	0.983	0.20 ± 0.26	0.068 ± 0.087
7.379	1.212	15.540	0.979	0.21 ± 0.19	0.070 ± 0.065
7.366	1.268	15.511	0.976	0.09 ± 0.15	0.030 ± 0.052
7.352	1.322	15.482	0.972	0.32 ± 0.17	0.110 ± 0.057
7.338	1.378	15.453	0.969	0.57 ± 0.19	0.195 ± 0.063
7.324	1.433	15.424	0.965	0.48 ± 0.17	0.164 ± 0.058
7.310	1.488	15.395	0.962	0.90 ± 0.21	0.306 ± 0.071
7.297	1.543	15.366	0.959	0.88 ± 0.20	0.299 ± 0.069
7.283	1.598	15.337	0.955	1.61 ± 0.26	0.549 ± 0.088
7.269	1.653	15.308	0.952	0.91 ± 0.20	0.311 ± 0.069
7.255	1.708	15.279	0.949	1.83 ± 0.27	0.626 ± 0.093
7.241	1.763	15.250	0.945	2.48 ± 0.31	0.85 ± 0.11
		$E = 18.356$ GeV		$\theta = 21.010°$	
7.908	1.185	19.302	0.984	0.013 ± 0.059	0.007 ± 0.032
7.883	1.295	19.240	0.979	0.155 ± 0.056	0.083 ± 0.030
7.857	1.405	19.177	0.973	0.274 ± 0.061	0.147 ± 0.033
7.832	1.515	19.115	0.968	0.384 ± 0.067	0.206 ± 0.036
7.806	1.625	19.053	0.962	0.334 ± 0.062	0.179 ± 0.033
7.781	1.735	18.991	0.957	0.466 ± 0.071	0.250 ± 0.038
7.755	1.845	18.929	0.952	0.769 ± 0.089	0.413 ± 0.048
		$E = 20.795$ GeV		$\theta = 21.010°$	
8.335	1.215	23.047	0.986	0.003 ± 0.029	0.002 ± 0.023
8.311	1.325	22.981	0.981	0.079 ± 0.034	0.062 ± 0.027
8.288	1.435	22.916	0.976	0.055 ± 0.028	0.043 ± 0.022
8.264	1.545	22.850	0.972	0.092 ± 0.032	0.072 ± 0.025
8.240	1.655	22.785	0.967	0.167 ± 0.040	0.130 ± 0.031
8.217	1.765	22.719	0.963	0.227 ± 0.045	0.177 ± 0.035
8.193	1.875	22.653	0.958	0.256 ± 0.048	0.200 ± 0.037
8.169	1.985	22.588	0.953	0.369 ± 0.057	0.287 ± 0.044
		$E = 21.182$ GeV		$\theta = 25.010°$	
6.735	1.235	26.754	0.987	0.006 ± 0.011	0.010 ± 0.017
6.716	1.345	26.679	0.983	0.017 ± 0.011	0.026 ± 0.017
6.698	1.455	26.605	0.979	0.043 ± 0.014	0.067 ± 0.022
6.679	1.565	26.530	0.975	0.078 ± 0.018	0.121 ± 0.027
6.660	1.675	26.455	0.971	0.056 ± 0.015	0.087 ± 0.023
6.641	1.785	26.381	0.967	0.060 ± 0.015	0.092 ± 0.023

Continued

Table I. Continued.

E' (GeV)	W^2 (GeV)^2	Q^2 (GeV/c)^2	x	$d\sigma/d\Omega dE'$ (pb/sr-GeV)	F_2 ($\times 10^3$)
		$E = 21.179$ GeV		$\theta = 33.010°$	
4.518	1.250	30.894	0.988	-0.002 ± 0.004	-0.009 ± 0.016
4.507	1.350	30.815	0.985	0.012 ± 0.006	0.044 ± 0.024
4.495	1.450	30.737	0.982	0.002 ± 0.004	0.006 ± 0.013
4.484	1.550	30.659	0.979	0.009 ± 0.006	0.035 ± 0.021
4.472	1.650	30.580	0.975	0.014 ± 0.006	0.053 ± 0.024
4.461	1.750	30.502	0.972	0.022 ± 0.008	0.081 ± 0.028
4.449	1.850	30.423	0.969	0.028 ± 0.009	0.105 ± 0.032
4.438	1.950	30.345	0.966	0.036 ± 0.009	0.132 ± 0.035

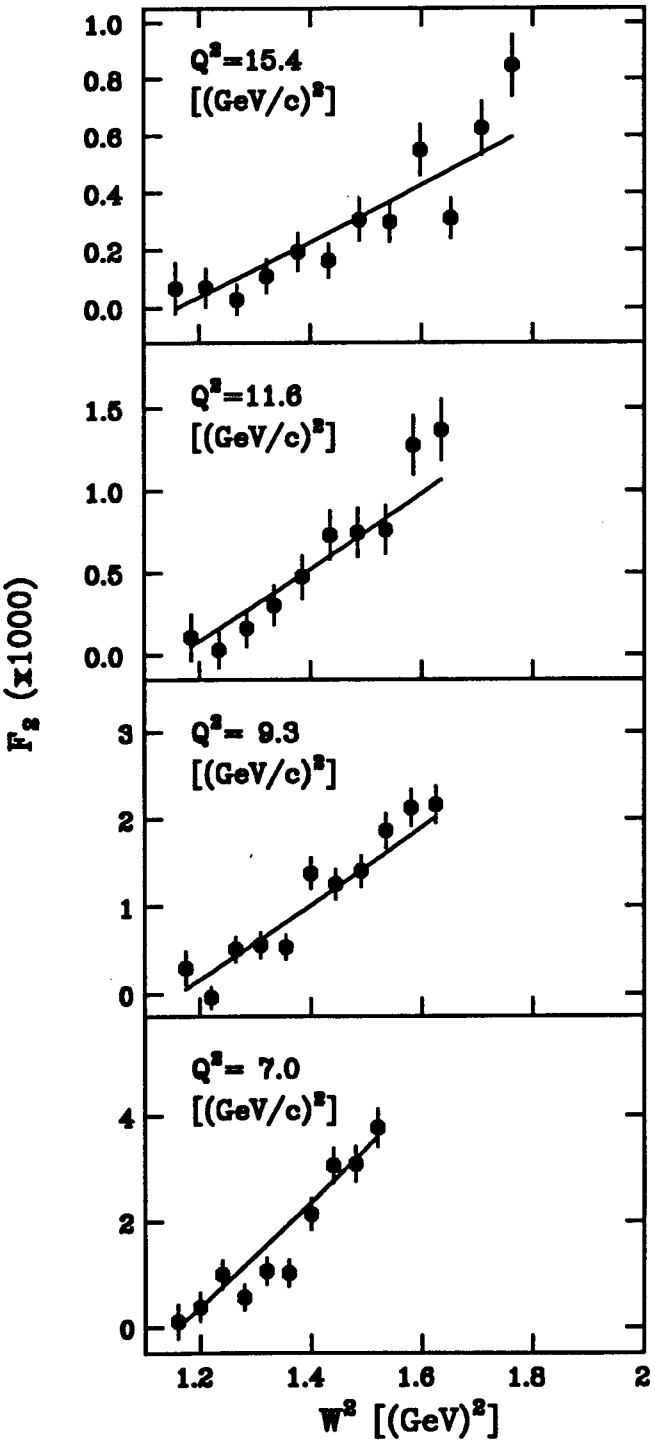
Q^2=15.4
[(GeV/c)^2]
Q^2=11.6
[(GeV/c)^2]
Q^2= 9.3
[(GeV/c)^2]
Q^2= 7.0
[(GeV/c)^2]
F_2 (x1000)
W^2 [(GeV)^2]

Fig. 1

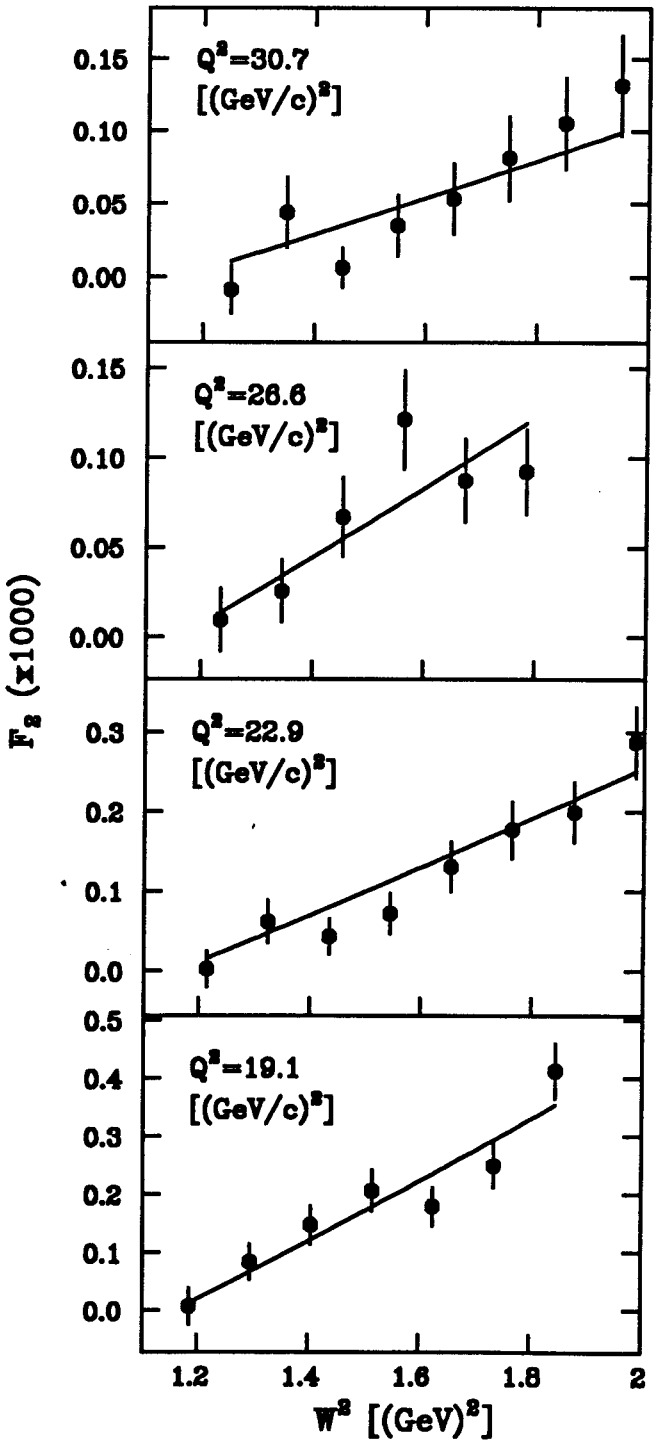
Q^2=30.7
[(GeV/c)^2]
Q^2=26.6
[(GeV/c)^2]
Q^2=22.9
[(GeV/c)^2]
Q^2=19.1
[(GeV/c)^2]
F_2 (x1000)
W^2 [(GeV)^2]

Fig. 2

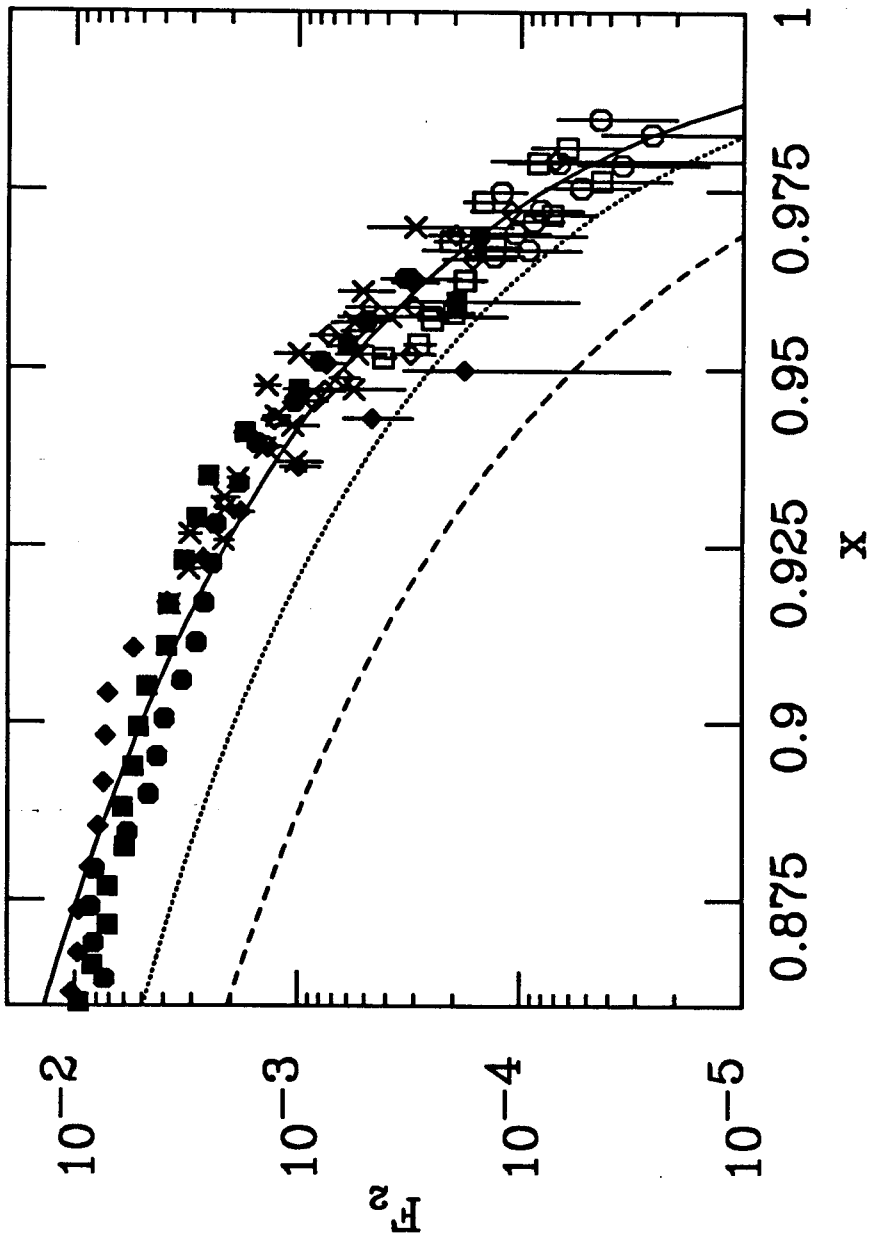

Fig. 3

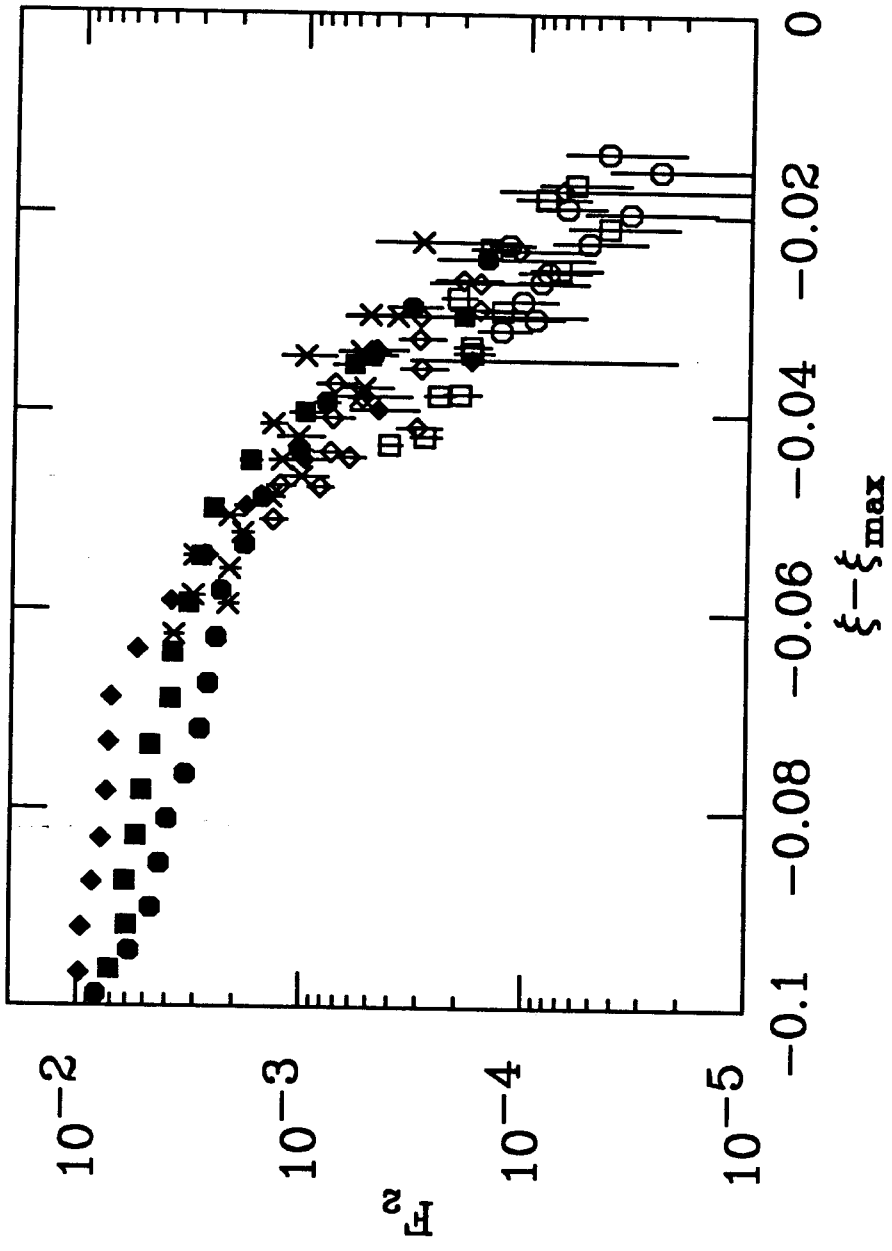

Fig. 4

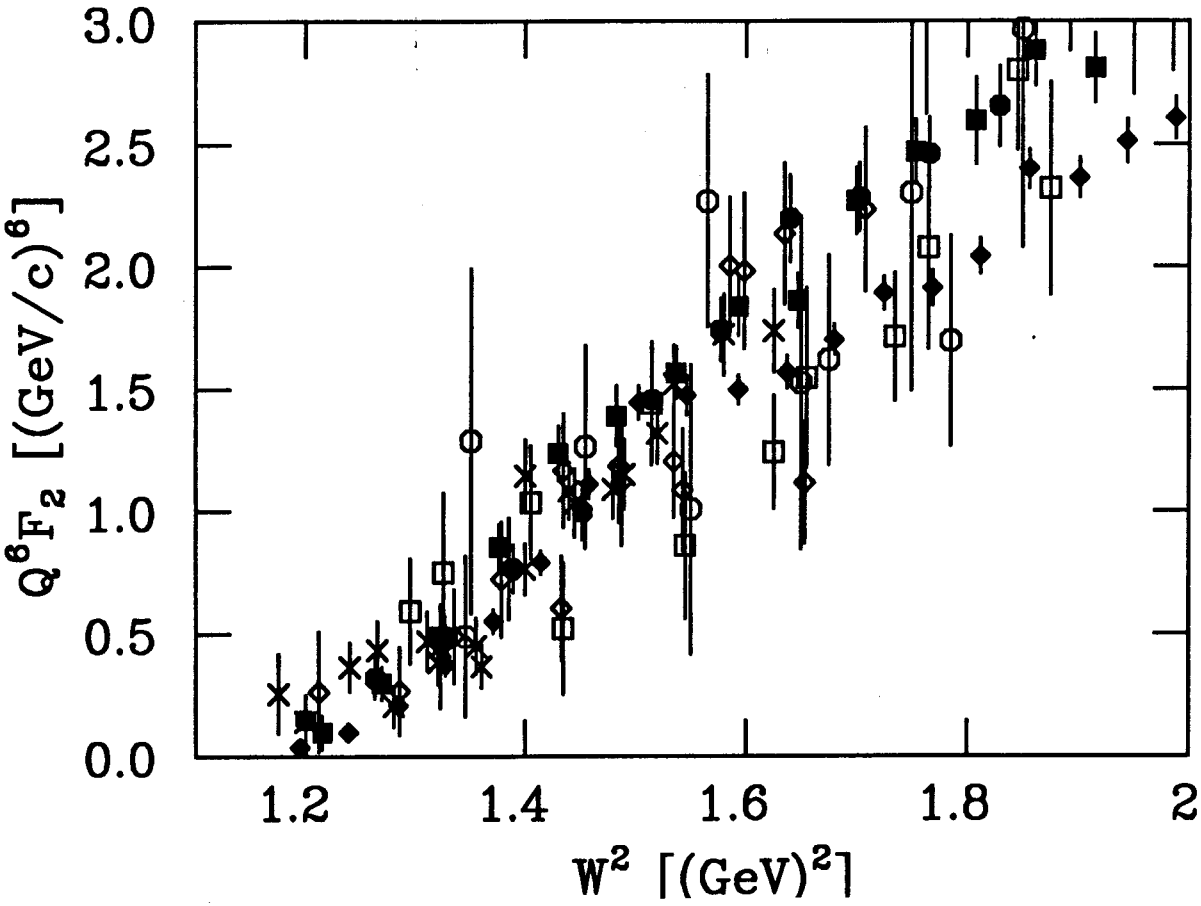

Fig. 5

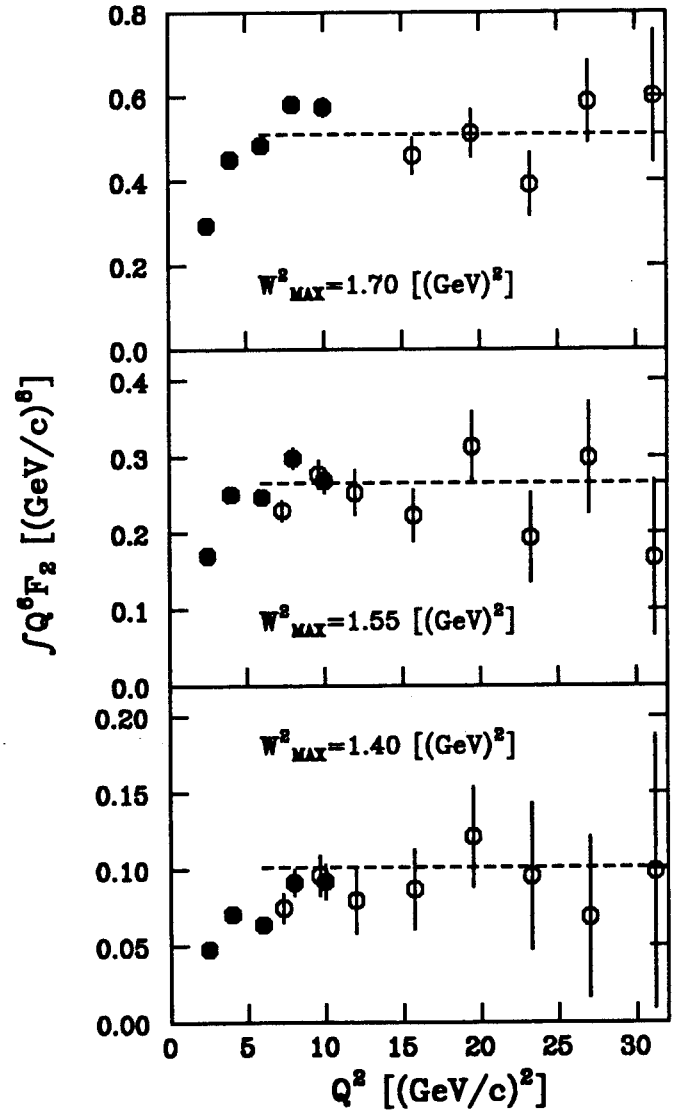
0.8
0.6
0.4
0.2
0.0
W^2_{MAX}=1.70 [(GeV)^2]
0.4
0.3
0.2
0.1
0.0
W^2_{MAX}=1.55 [(GeV)^2]
0.20
0.15
0.10
0.05
0.00
W^2_{MAX}=1.40 [(GeV)^2]
0
5
10
15
20
25
30
Q^2 [(GeV/c)^2]
$\int Q^6 F_2$ [(GeV/c)^6]

Fig. 6